JOURNAL OF GEOPHYSICAL RESEARCH, VOL. 112, B06405, doi:10.1029/2005JB003941, 2007

Viscosity structure of the crust and upper mantle in western Nevada from isostatic rebound patterns of the late Pleistocene Lake Lahontan high shoreline

Bruce G. Bills,[1,2] Kenneth D. Adams,[3] and Steven G. Wesnousky[4]

Received 13 July 2005; revised 26 October 2006; accepted 31 January 2007; published 8 June 2007.

[1] Large lakes can both produce and record significant crustal deformation. We present an analysis of the isostatic rebound pattern recorded in the shorelines of paleolake Lahontan, in western Nevada, using a layered Maxwell viscoelastic model. The inferred viscosity structure depends on loading history. We use three variants of a well-documented lake surface elevation model as input and recover corresponding estimates of viscosity and density structure. A simple two-layer model, with an elastic plate over an inviscid half-space, fits the observed elevation pattern quite well, with a residual variance of 32% of the data variance. Using multilayered, finite viscosity models, the residual variance is reduced to 20% of the data variance, which is very near to the noise level. In the higher-resolution models, the viscosity is below 10^{18} Pa s over the depth range from 80 to 160 km. The minimum viscosity is very similar to the value that has been seen in the eastern Great Basin, from similar analyses of Lake Bonneville shorelines, but the low-viscosity zone is thinner beneath Bonneville. Making small adjustments to a seismically derived density structure allows an improved fit to the shoreline observations. Additionally, we find that small variations in proposed loading models can result in presumably spurious density inversions, and suggest that this modeling approach provides a test for loading histories.

Citation: Bills, B. G., K. D. Adams, and S. G. Wesnousky (2007), Viscosity structure of the crust and upper mantle in western Nevada from isostatic rebound patterns of the late Pleistocene Lake Lahontan high shoreline, *J. Geophys. Res.*, *112*, B06405, doi:10.1029/2005JB003941.

1. Introduction

[2] Large lakes provide an opportunity to examine the long-term strength of the rock on which they are supported. A sufficiently large lake can both produce and record significant crustal deformation. The spatiotemporal pattern of that deformation is diagnostic of the strength of the crust and upper mantle in the region below the lake. The objective of this paper is to examine the deformation recorded in the pattern of elevation variations on the highest shoreline of late Pleistocene Lake Lahontan, in western Nevada, and use it to derive estimates of viscosity structure in the tectonically active western Great Basin.

[3] Lacustrine shorelines form as essentially level surfaces and are produced whenever the lake surface elevation is stable for a long enough time to allow wave energy to modify the shore zone configuration. When the lake is deep, the weight of water in it deflects the crust downward by an amount which depends on the density, rigidity, and viscosity of the substrate, and the depth, density, and lateral extent of the water load. When the lake level drops, the crust rebounds and the shorelines are deflected upward in the basin center. By measuring the present-day departure from horizontality along a single shoreline, we have an indication of differential vertical motion since the shoreline formed. If, in addition, the age of the shoreline is known, and the lake level history and current basin topography are known well enough to reconstruct the entire spatiotemporal loading pattern, then the long-term effective strength of the Earth, in that region, can be inferred.

[4] On short timescales, the mechanical behavior of the crust and mantle are well approximated by an elastic solid. On long timescales, most of the nominally solid Earth behaves much like a viscous fluid. An important objective of geodynamics research is characterizing this transition from solid-like to fluid-like behavior and mapping the effective viscosity variations throughout the crust and mantle. Much of what is currently known about these viscosity variations has been inferred from patterns of marine shoreline deformation associated with major glaciations [*Peltier*, 1998; *Kaufmann and Lambeck*, 2000; *Mitrovica et al.*, 2001; *Peltier et al.*, 2002].

[5] The information provided by shoreline patterns of large lakes complements global glaciomarine investigations in several ways. In both cases, it is necessary to know the

[1] NASA Goddard Space Flight Center, Greenbelt, Maryland, USA.
[2] Scripps Institution of Oceanography, La Jolla, California, USA.
[3] Desert Research Institute, Reno, Nevada, USA.
[4] Center for Neotectonic Studies, University of Nevada, Reno, Nevada, USA.

0148-0227/07/2005JB003941$09.00

current elevations and ages of the shorelines and the history of loading. The marine shorelines are obviously limited to continental margins and oceanic islands, whereas lakes often occur in continental interiors. Reconstructing the detailed geometry of the loads is easier for lakes than for the continental ice sheets.

[6] One of the primary challenges in using the marine shoreline record is that the global pattern of sea level variations is quite complex, and shoreline chronologies are all essentially local, or at best, regional. In contrast, the highest shoreline of a large paleolake can often be traced in a nearly continuous fashion around the perimeter of the basin and on mountain ranges which were formerly islands within the lake. In that regard, the geometry and history of the shorelines are more nearly separable in the lacustrine environment than in the marine record. Though challenging, both the absolute ages of the lacustrine shorelines and their synchroneity of formation can often be established around the entire perimeter of lakes [*Adams and Wesnousky*, 1998, 1999].

[7] Lake Lahontan was a large, late Pleistocene lake in the westernmost part of the Great Basin region of Nevada and Utah. It was essentially contemporaneous with Lake Bonneville, which occupied the easternmost part of the Great Basin. Scientific studies of the shorelines, sediments, and hydrologic histories of lakes Lahontan and Bonneville were started at nearly the same time [*Russell*, 1885; *Gilbert*, 1890], but the rebound pattern on the shorelines of Lake Bonneville was appreciated much earlier [*Gilbert*, 1890; *Crittenden*, 1963] mainly because of the fact that the signal there is much larger. The Bonneville shoreline pattern [*Currey*, 1982] and loading history [*Oviatt and Thompson*, 2002] have been subsequently refined and have been frequently used to derive estimates of crust and upper mantle viscosity [*Crittenden*, 1963; *Passey*, 1981; *Iwasaki and Matsuura*, 1982; *Nakiboglu and Lambeck*, 1982, 1983; *Bills and May*, 1987; *Bills et al.*, 1994a, 2002]. In contrast, the Lahontan rebound signal has received relatively little study [*Mifflin and Wheat*, 1971, 1979; *Mifflin*, 1984] until recently [*Adams et al.*, 1999], despite the fact that considerable work has been done on the lake level history there [*Morrison*, 1964, 1991; *Benson and Thompson*, 1987; *Benson et al.*, 1991, 1992, 1995, 1996; *Bradbury et al.*, 1989; *King*, 1993; *Adams and Wesnousky*, 1998].

[8] Many previous studies have used water loads, either in the form of artificial filling of reservoirs or the natural fluctuation of lake levels, to probe the response of the crust to these loads. The filling of Lake Mead, on the Colorado River, with 35 km^3 of water caused about 0.2 m of subsidence [*Kaufmann and Amelung*, 2000]. Filling of La Grande reservoir in Quebec with 60 km^3 of water caused about 0.1 m of subsidence [*Lambert et al.*, 1986]. The anticipated filling of the Three Gorges Reservoir on the Yangtze river in China is expected to cause about 0.1 m of subsidence [*Zhang et al.*, 1996; *Wang*, 2000; *Wang et al.*, 2002]. The filling of the Salton trough in southern California, via natural diversions of the Colorado river, to form Lake Cahuilla [*Waters*, 1983; *Sturm et al.*, 1996; *Buckles et al.*, 2002], with a maximum depth of 95 m and volume of 280 km^3, produced about 0.4 m of subsidence [*Larson*, 1990].

[9] Much larger crustal deformation responses are recorded in the shorelines of some larger paleolakes. Among late Pleistocene lakes with at least partially known deformation patterns, we mention Lake Minchin, in Bolivia [*Argollo and Mourguiart*, 2000; *Fornari et al.*, 2001; *Baker et al.*, 2001], which had a maximum volume of 5000 km^3 and produced 30 m of subsidence [*Bills et al.*, 1994b], and Lake Bonneville in Utah, with a maximum volume of over 9000 km^3 and peak subsidence of 70 m (see references above).

[10] A number of other large Pleistocene paleolakes are known, but for most of them, the isostatic response signal recorded in their shoreline elevation patterns has not yet been investigated. Of the possibly large number of such lakes that deserve further study, we mention only two. Lake Chad, in west central Africa, occupies a basin which formerly contained a much larger lake. Estimates of the maximum extent of the former lake vary [*Olivry et al.*, 1996; *Kutzbach*, 1980; *Ghienne et al.*, 2002], but it appears likely to have been in excess of 10^4 km^3. The northwest corner of Mongolia contains several large shallow lakes, all of which are surrounded by higher shorelines. The timing and maximum former extent of these lakes is still only poorly constrained [*Komatsu et al.*, 2001; *Grunert et al.*, 2000; *Lehmkuhl and Lang*, 2001; *Lehmkuhl and Haselein*, 2000; *Peck et al.*, 2002] but it appears likely that during the late Pleistocene there was sufficient water in these lakes to produce significant crustal deformation.

[11] The fortuitous occurrence of two large paleolakes, Bonneville and Lahontan, in close proximity within the Great Basin provides a unique opportunity to look for lateral variations in viscosity structure. Previous work on the Bonneville rebound pattern has shown that the upper mantle viscosity in that region is much lower than has been inferred from global-scale glacial rebound studies. A plausible explanation for that difference is that the upper mantle beneath the Great Basin is hotter than the global average. That interpretation is well supported by observations of high heat flow [*Lachenbruch*, 1978], recent volcanism [*McKee and Noble*, 1986], and extensional tectonics [*Minster and Jordan*, 1987; *Zoback*, 1989; *Dixon et al.*, 1995; *Bennett et al.*, 1998]. *Dixon et al.* [2004] have argued that small amounts of water in the mantle can also play an important role in determining viscosity. In the western United States, low viscosity in the upper mantle thus likely reflects the combined effect of elevated temperature and high water concentration associated with Farallon plate subduction. For a recent review of the geophysical structure of this region, see the work of *Humphreys and Dueker* [1994a, 1994b].

[12] Pursuing this notion further, one might anticipate that the viscosity beneath Lake Lahontan would be even lower than beneath Lake Bonneville, based on the patterns of heat flow, magmatic activity, gravity/topography coherence [*Lowry and Smith*, 1994, 1995], and isotopic patterns [*Farmer and Ball*, 1997; *DePaolo and Daley*, 2000]. Careful study of the deformation pattern recorded in the Lahontan shorelines provides an opportunity to determine whether the viscosity structure differs significantly between the eastern and western portions of the Great Basin.

[13] The motivation for the present study has several components. The pattern of rebound on the Lake Lahontan shorelines has only recently been delineated [*Adams et al.*, 1999], and no proper analysis of that pattern, in terms of viscosity structure, has yet been presented. We wish to

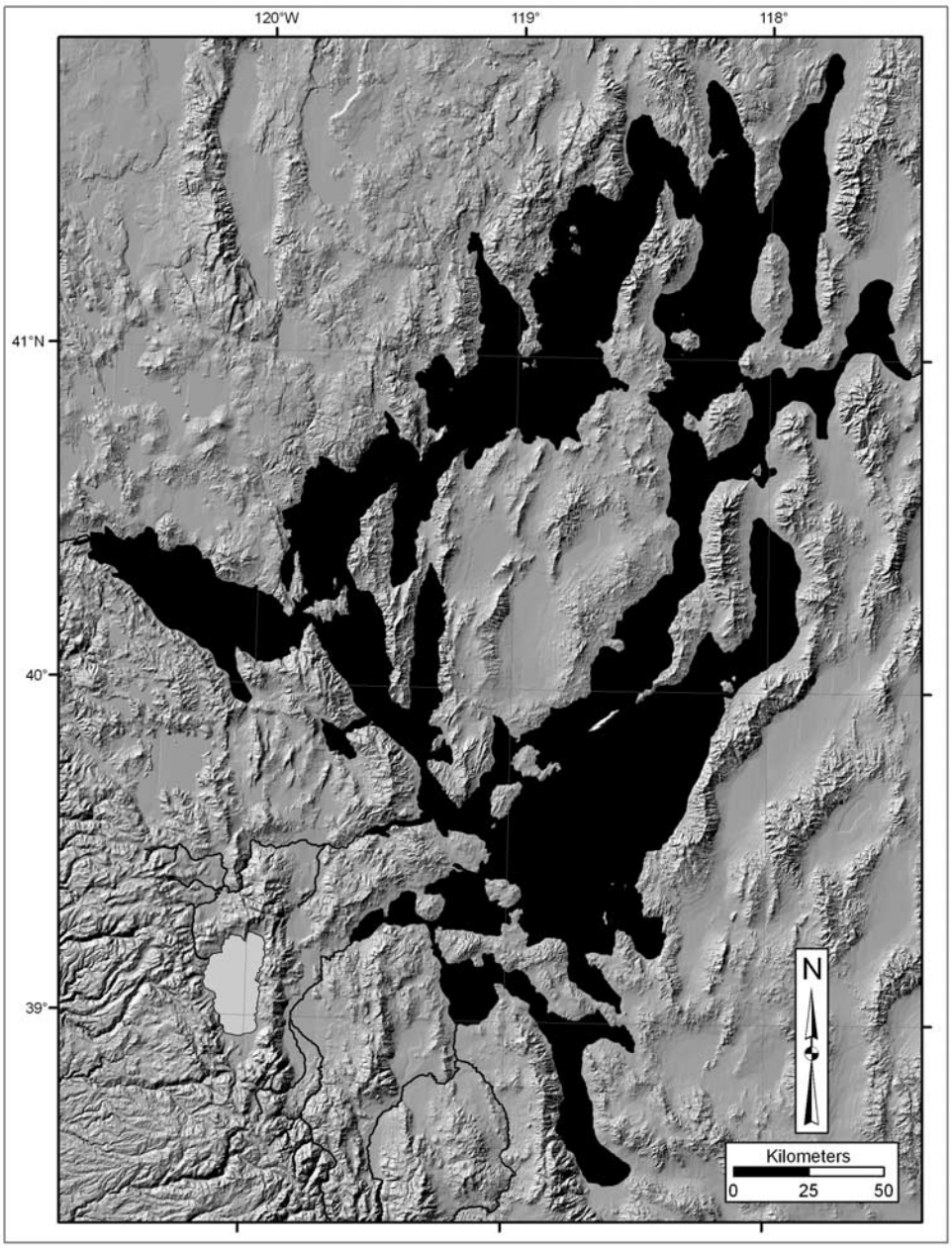

Figure 1. Location of Lake Lahontan. The lake configuration was reconstructed using a present-day surface elevation of 1332 m.

compare the regional solution for viscosity structure in western Nevada with other inferred viscosity models; both global solutions derived from marine shorelines, and regional models derived from the relatively nearby paleo-lake Bonneville, in western Utah. We also have a new solution algorithm in which both density and viscosity are adjusted. Small adjustments to the initially assumed density structure largely remove long wavelength residual patterns which were problematic in previous analyses of Lake Bonneville rebound patterns [*Bills and May*, 1987; *Bills et al.*, 1994a, 2002].

[14] The remainder of the paper is divided into four sections. Section 2 discusses the observations, which consist of the spatial pattern of elevations on the highest shoreline of Lake Lahontan, and the temporal variations in water depth. Section 3 presents an initial attempt to model the observed rebound pattern in terms of a simple elastic model. Section 4 presents the results and implications of our viscoelastic modeling. Section 5 presents our discussion and conclusions.

2. Observations

[15] The primary observational constraints on our models are the pattern of shoreline elevations, the present basin topography, and the history of the water surface fluctuations. The latter two are used to reconstruct the load, which is the basic input to the deformation process. The shoreline elevations represent the output, and our model of the physical process has adjustable parameters which we con-

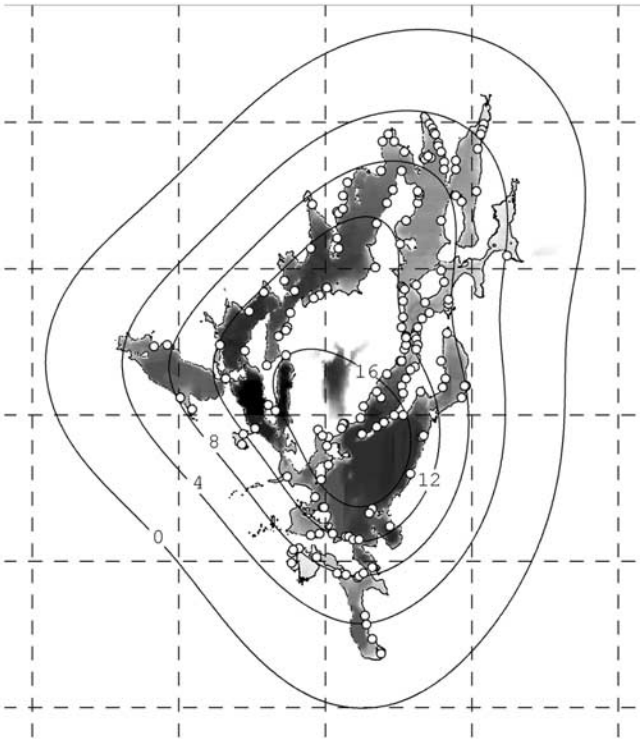

Figure 2. Rebound pattern on highest shoreline of Lake Lahontan. Grid spacing is 50 km. Dots indicate locations of shoreline points surveyed by *Adams et al.* [1999]. Gray level indicates water depth variations. Contours depict the response of an elastic plate on a fluid substrate with parameters obtained by fitting to the observed shoreline elevation pattern. Contour interval is 4 m.

strain by making the model output match the observed shoreline elevations.

2.1. Basin Topography

[16] The present basin topography is quite adequately known, for purposes of reconstructing the water load. Recent digital elevation models, such as the National Elevation Data Set (NED) Model compilation, and the data from the Shuttle Radar Topography Mission (SRTM), provide a level of resolution and fidelity which may allow automated shoreline elevation pattern extraction, as has been proposed by *Hare et al.* [2001]. However, for the present, we use a 30-arcsecond-resolution digital elevation model (GTOPO30), interpolated to a 1 × 1 km grid in the Universal Transverse Mercator (UTM) coordinate system. That provides a locally Cartesian coordinate frame. We have chosen an arbitrary local coordinate origin at 40°N, 119°W, which corresponds to UTM coordinates of E = 329,270 m and N = 4,429,463 m in zone 11.

[17] Figure 1 illustrates an approximate reconstruction of the maximum extent of Lake Lahontan. This first approximation was obtained by simply flooding the present topography below an elevation of 1332 m. That gives a good initial estimate of the outline of the lake, but completely ignores the isostatic rebound signal, which is the primary focus of the current investigation. A better approximation could be obtained by subtracting a smoothed representation of the rebound pattern, as shown in Figure 2, from the present topography, and flooding it. However, in most places around the basin, the intersection of the water surface with the landscape is influenced rather little by the correction. Quite similar depictions of the extent of Lake Lahontan and other adjacent lakes are given by *Mifflin and Wheat* [1979] and *Reheis* [1999a, 1999b].

[18] Figure 3 illustrates the drainage basin of Lake Lahontan. At low water levels, each of several subbasins contained an independent lake. As water level rose, the sills or divides separating them were submerged and the adjacent basins became integrated into successively larger lakes. In addition to the subbasins which were fully assimilated into Lake Lahontan, as the water level rose, there were two distal basins which contributed significant overflow but did not become part of the lake proper. On the western margin of the basin, Lake Tahoe was exporting significant amounts of water during most of the last pluvial lake cycle. On the eastern margin of the basin, Lake Diamond exported significant water during the period when it was overflowing and downcutting its outlet from 1824 to 1775 m [*Tackman*, 1993].

[19] These distal basins were an integral part of the hydrologic entity comprising Lake Lahontan but were small enough in mass and far enough away from the center that we will ignore their geodynamic contributions. Other nearby lakes, such as the one in Dixie Valley, were hydrologically separated from Lake Lahontan, but likely contributed somewhat to the deformation pattern within the Lahontan domain. However, we will also ignore these effects. *Caskey and Ramelli* [2004] have measured elevations of the highest shorelines in Dixie valley, and note that the deformation pattern seen on them is concordant with the pattern projected from nearby portions of Lake Lahontan.

2.2. Shoreline Elevations

[20] The shoreline elevation pattern described by *Adams et al.* [1999] will be used as our primary geometrical constraint on the response to surface loading. Figure 2 illustrates a smoothed representation of the shoreline elevation pattern, obtained by using an elastic plate model, which will be described in more detail below.

[21] The error in the elevation measurements deserves some comment. Because of a high density of good-quality vertical control points in the region, it is not particularly difficult to measure the elevation of a point with an accuracy of 10 cm. Measurement error per se is not an issue. However, local variations in the height of features associated with the shoreline of interest are typically 1–2 m [*Adams and Wesnousky*, 1998]. Among the sources of beach height variation, relative to the still water level at the time of formation, are sediment source and supply [*Carter and Orford*, 1988], particle size and shape [*Bluck*, 1967; *Williams and Caldwell*, 1988], wave runup [*Kirk*, 1975; *Forbes et al.*, 1991], and rate of lake level change [*Dillon*, 1971; *Kirk*, 1980; *Orford et al.*, 2002]. Other sources of variation are discussed, at some length, by *Adams and Wesnousky* [1998] and *Hare et al.* [2001]. We assume that 2 m is a representative error in reconstruction of the rebound pattern from measurements of the present shoreline elevations. A challenge for the modeling exercise is to reproduce the observations to that level of accuracy.

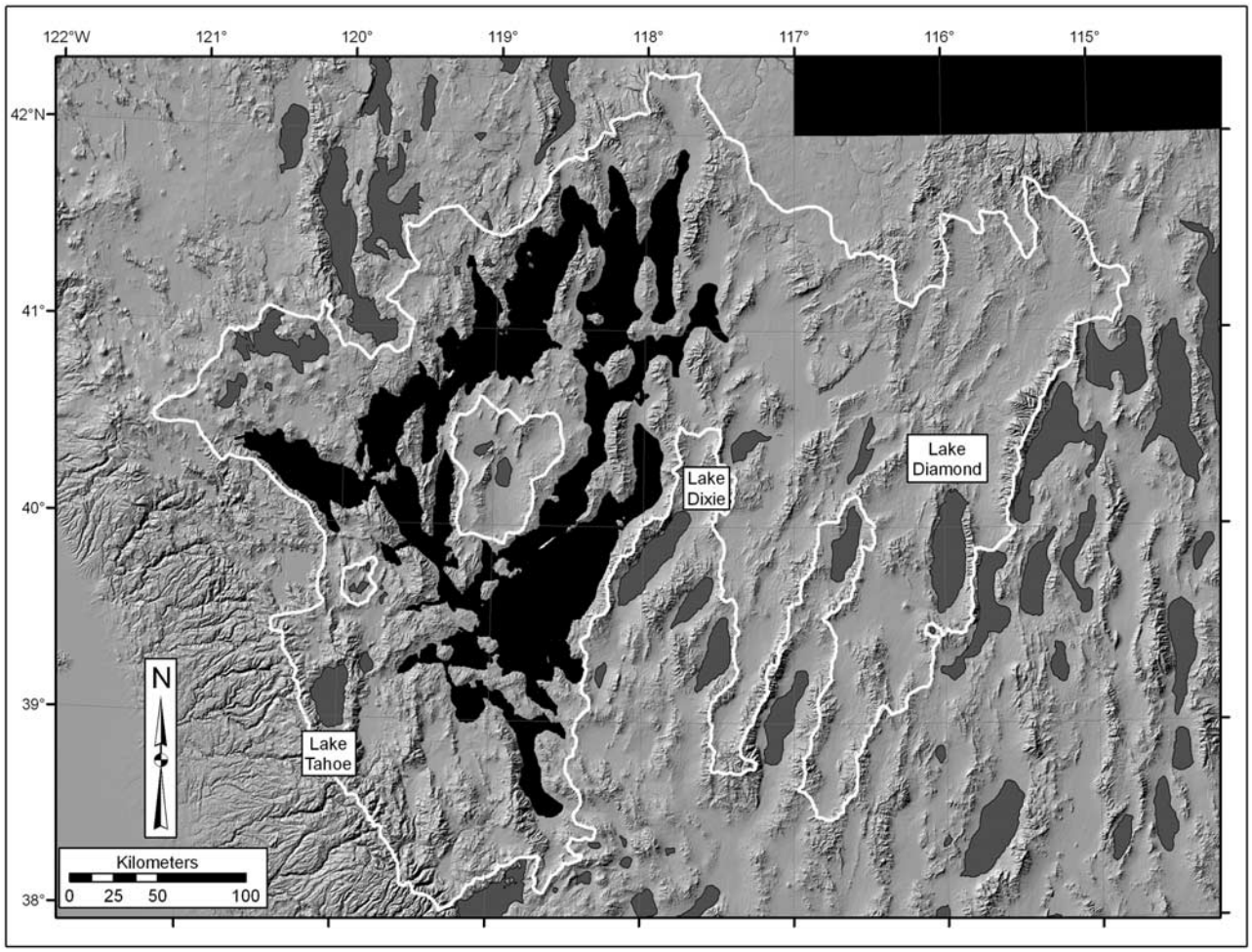

Figure 3. Lake Lahontan drainage basin, with major subbasins indicated. Black indicates Lake Lahontan. Dark gray indicates other late Pleistocene lakes in the vicinity.

2.3. Lake Level History

[22] The major observational challenge in geodynamic paleolake studies is reconstructing the history of lake surface elevation fluctuations. Because those fluctuations are of interest for a variety of other applications, considerable effort has been devoted to understanding Lake Lahontan history, but many important aspects of the history are still far from clear. During historic times, the hydrologic balance fluctuations in the eastern and western extremities of the Great Basin, where lakes Bonneville and Lahontan formerly resided, have been quite similar. Likewise, the major lake level fluctuations in the two largest paleolakes of the Great Basin also appear to have been generally quite similar.

[23] In terms of basic geography, the Lahontan and Bonneville basins share many characteristics, with low broad plains in the valley bottoms, and relatively steep slopes on the surrounding mountains. As each lake grew in depth, several initially independent smaller lakes merged to form a single larger lake. However, the geomorphology of the Lahontan basin differs from that of Bonneville in an important way, which is partially illustrated in Figure 4a and 4b. That figure contrasts the variations of surface area and water volume with depth for the two basins. Bonneville attains a significant fraction of its maximum total surface area at a relatively shallow depth, whereas Lahontan gains fractional area more slowly at the beginning of infilling.

[24] Within the past few decades, the lowest exposed point in the Lahontan basin has been the lowest point in Poito (Winnemucca) valley (near 40.2°N, 119.3°W) at 1148 m. The surface of Pyramid Lake (39.8–40.2°N, 119.3–119.7°W) was as low as 1153 m in the summer of 1967 and has been near 1160 m for the past few years. Pyramid Lake is quite deep, with a low point near 1040 m, but the volume contained below the current surface level is relatively small ($\sim$29 km^3) and is ignored in subsequent discussions.

[25] Another result of the differing basin configurations is that Lahontan only functioned as a single large lake over the upper $\sim$20 m of its $\sim$150-m elevation range, whereas Bonneville was a single large lake over much more of its history. When all the constituent basins are joined as a single lake, observations on lake level timing in one basin apply to all other subbasins. However, at the lower levels, the separate smaller lakes operate quite independently. As a result, reconstructing the Lahontan lake-level history is intrinsically more difficult than for Bonneville.

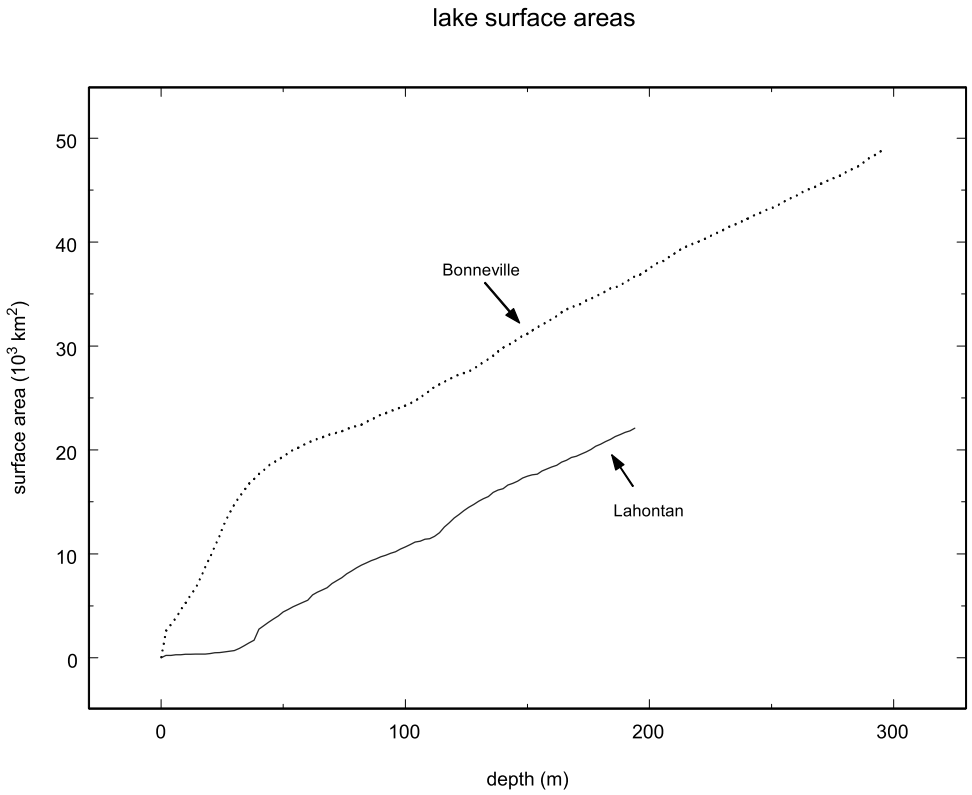

Figure 4a. Lake surface area versus depth for lakes Lahontan and Bonneville.

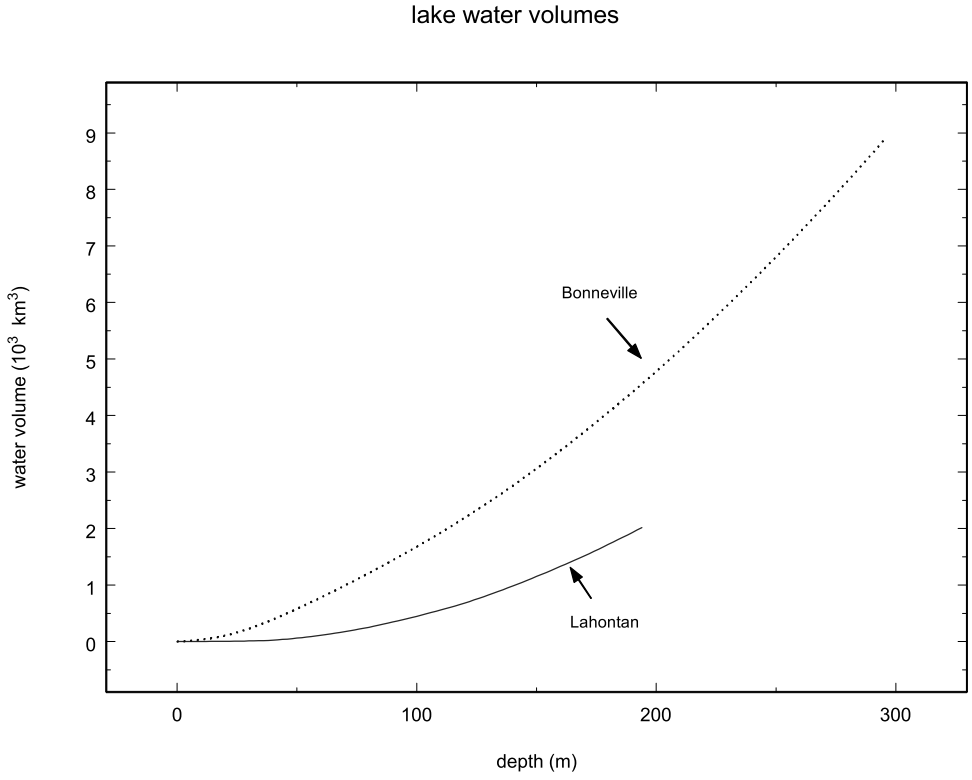

Figure 4b. Lake water volume versus depth for lakes Lahontan and Bonneville.

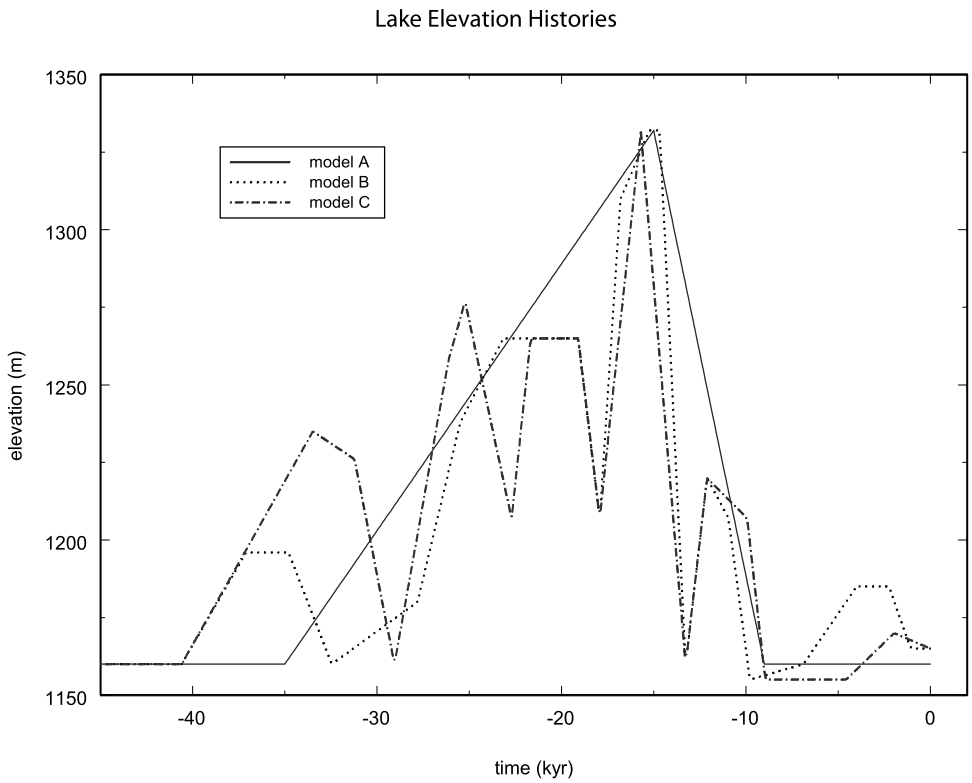

Figure 5. Lake level histories used in computing viscoelastic response. See text for descriptions.

[26] Another minor complication in using these loading histories is that the associated ages are reported in terms of radiocarbon years, rather than calendar years. If the transformation were merely a linear change of scale, the only error associated with using the uncorrected times would be that the estimated viscosities would be uniformly wrong by the conversion factor. Over much of the past 20 kyr the error would only be 10–20%, which is smaller than the uncertainty of our viscosity estimates. However, the actual time transformation is rather more complex, and failure to convert to calendar years would change the relative durations of various parts of the loading history and could produce serious errors in recovered Earth structure. We use the compilations of *Stuiver et al.* [1998] and *Beck et al.* [2001] to convert the reported radiocarbon ages of lacustrine events into calendar ages.

[27] For present purposes, we will examine the geodynamic consequences of three different lake level models. Model B is based on the work of *Benson et al.* [1995] and will be our baseline model. Model C is rather similar and will be described in detail below. Model A is the simplest of the three and has a linear increase in water depth from −30 to −15 kyr, a linear decrease from −15 to −9 kyr, and essentially no load at other times. These three lake level models are compared in Figure 5. For most of our analyses, we will ignore the low-elevation multiple basin complexity just discussed and operate on the assumption that a single lake-surface elevation trajectory is adequate.

[28] In Figure 6a and 6b, we present trajectories of lake surface area and lake volume versus time corresponding to the three lake surface elevation curves which will be used in the subsequent modeling. These were constructed from the elevation trajectories in Figure 5, along with the elevation-versus-area and elevation-versus-volume curves for the Lahontan basin, as shown in Figure 4. Though these curves are in error, at low elevations, because of the neglect of separate lakes in each subbasin, the curves do illustrate the fact that much of the volume-time product, which is the quantity most relevant to the deformation response, comes from the episodes when the lake was near maximum elevation, and the curves should adequately represent the actual load history during those intervals.

[29] The lake level history C differs from history B in several significant ways, including the timing, duration, and magnitude of several fluctuations. The peak between about −35 and −30 kyr on curve C is constrained by the presence of the Wono tephra (27,300 ^{14}C yr B.P. [*Benson et al.*, 1997]) in offshore sands at an elevation of about 1220 m at the north end of Winnemucca Lake (Adams, unpublished notes) and at about 1210 m in the Black Rock Desert (BRD) [*Davis*, 1985]. After that peak, lake level descends to a low stand referred to as the Wizard's Beach recession [*Dansie et al.*, 1988].

[30] At the time of deposition of the Trego Hot Springs (THS) bed (23,200 ^{14}C yr B.P. [*Benson et al.*, 1997]), the lake was rising through an elevation of about 1258 m and reached at least 1275 m shortly thereafter [*Davis*, 1983]. The THS bed is found in an aggrading delta at about 1258 m [*Davis*, 1983] and in beach deposits at about 1250 m in the BRD [*Davis*, 1987]. This conflicts with the interpretation by *Benson et al.* [1997] that lake level was at or below 1177 m when the THS bed was deposited.

[31] The drop in lake level between −23 and −22 kyr is based on stratigraphic exposures in the BRD which suggest a recession to or below 1210 m during the interval from

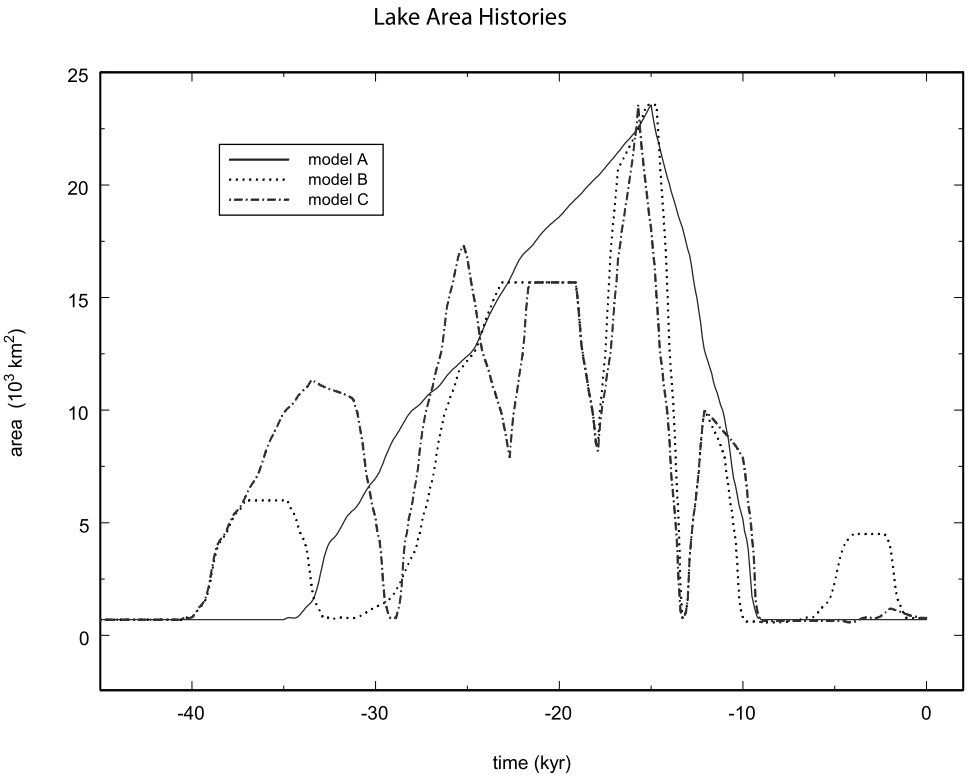

Figure 6a. Lake surface area versus time for Lake Lahontan surface elevation histories of Figure 5.

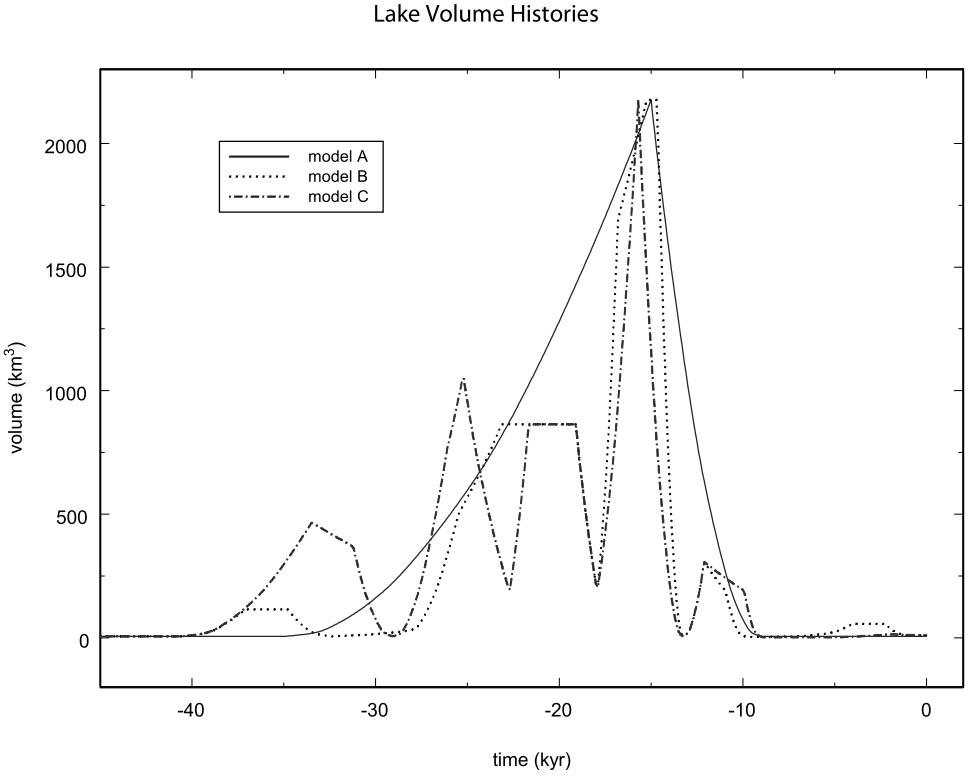

Figure 6b. Lake water volume versus time for Lake Lahontan surface elevation histories of Figure 5. Increase in basin volume due to deformation has been ignored in this figure.

−25 to −20 kyr, though its exact timing is not yet known (Adams, unpublished notes). In model C, the late Pleistocene highstand occurred at about −15,700 kyr (13,070 ^{14}C yr B.P. [*Adams and Wesnousky*, 1998]) and only lasted years to a decade or two. Lake-level fluctuations since the highstand are based on the work of *Born* [1972], *Benson et al.* [1992], and *Briggs et al.* [2005].

3. Elastic Plate Model

[32] Obtaining a model which yields a good fit to the observations is only part of the problem. We also want to be able to interpret the model. In this section, we illustrate that a very simple model can be used to obtain a reasonably good fit to observations. The model we use for this purpose consists of a thin elastic plate buoyantly supported by a dense fluid substrate. This model serves several purposes. It will illustrate the point that even a very simple physical model can often represent the outcome of much more complicated processes. It also provides a benchmark against which we can compare the performance of the more complex models we will subsequently develop. Part of the motivation for this particular model is that it approximates the long-term behavior of a viscoelastic model in which the viscosity decreases with depth.

[33] An advantage of this simple model is that it yields a linear relationship between applied water load and resulting crustal deformation pattern and thus requires no knowledge of the history of lake level fluctuations. A problem with the model is that it cannot be easily interpreted. For example, separate shorelines in the same lake basin need not yield the same set of parameters, since a longer duration load on a viscoelastic substrate will allow more of the substrate to relax and the effective plate thickness will decrease with time.

[34] The load P, or vertical force per unit area, associated with a lake water depth $d(x, y)$ is just

$$P(x,y) = \rho_w g d(x,y) \tag{1}$$

where ρ_w is the water density, and g is the acceleration due to gravity. We will assume values of

$$\begin{aligned} \rho_w &= 1000 \text{ kg m}^{-3} \\ g &= 9.8 \text{ ms}^{-2} \end{aligned} \tag{2}$$

The force balance for a thin elastic plate on a fluid substrate can be written as [*Timoshenko and Woinowsky-Krieger*, 1959; *Watts*, 2001]

$$\rho_s \, g \, w + D \, \nabla^4 w = P \tag{3}$$

where ρ_s is the density of the substrate, D is a plate flexural parameter, and w is the vertical deflection of the plate. The substrate responds only buoyantly, and the plate responds only via bending. The plate flexural parameter depends on the thickness h, elastic rigidity μ, and Poisson's ratio ν of the plate according to

$$D = \frac{\mu h^3}{6(1-\nu)} \tag{4}$$

We will initially assume values of

$$\mu = 32 \text{ GPa} \tag{5}$$

$$\nu = 0.5 \tag{6}$$

and let the plate thickness h vary. However, it is the parameter D which actually controls the response of the model.

[35] An important feature of this model is that the roles of the buoyant and flexural components are quite separable. The basic support mechanism is buoyancy, and, from Archimedes' principle, we expect that the displaced mass is equal to the load mass. The total displaced volume depends only on the volume of the load and the density ratio of the load and substrate. If the elastic plate has no strength, the deflection of the surface exactly mirrors the load and it would be in a state of local isostatic balance. Increasing the flexural strength of the elastic plate spreads the displacement over a larger area but decreases the amplitude in such a way that the displaced volume remains constant.

[36] The simplest way to solve these differential equations is via Fourier transforms. The Fourier transform of a spatial function $f(x, y)$ will be denoted by an overbar ($f \rightarrow \bar{f}$) and is obtained via the integral

$$\bar{f}(k_x, k_y) = \int_{-\infty}^{\infty} \int_{-\infty}^{\infty} f(x,y) e^{i(k_x x + k_y y)} \, dx dy \tag{7}$$

where wave numbers, or spatial frequencies, in the x and y coordinate directions are denoted k_x and k_y, respectively. A Fourier transform converts differential equations to algebraic equations and converts the operation of convolution to simple multiplication. Spatial patterns are thus represented by amplitude and phase at each spatial frequency, and the effect of the substrate and plate on the imposed load is represented by a Fourier-domain filter $\bar{F}$, which converts input (load) to output (surface deformation). We can write the transformed version of the force balance for our floating plate model as

$$\left(\rho_s g + D k^4\right) \bar{w} = \rho_w g \bar{d} \tag{8}$$

where we have used the notation

$$k^2 = k_x^2 + k_y^2 \tag{9}$$

This algebraic equation relating water depth to deformation can be solved in the form

$$\bar{w} = \bar{F}(a, b, k_x, k_y) \bar{d} \tag{10}$$

where the filter F has the form

$$\bar{F}(a, b, k_x, k_y) = \frac{1}{a + b^4 k^4} \tag{11}$$

and the filter parameters are

$$a = \frac{\rho_s}{\rho_w} \tag{12}$$

$$b = \left(\frac{D}{\rho_w g}\right)^{1/4} \tag{13}$$

This is effectively a low-pass spatial filter. At low spatial frequencies, the buoyant response of the substrate dominates, and the deformation is just a scaled version $(1/a)$ of the input load. At high spatial frequencies, the flexural response of the plate dominates, and the deformation is attenuated. The transition spatial frequency k_t, at which buoyant and flexural effects are equal, is given by

$$a = b^4 k_t^4 \tag{14}$$

The parameter a is dimensionless, and the parameter b is dimensionally a length. The transition wavelength λ_t is related to the filter parameters via

$$\lambda_t = \frac{2\pi}{k_t} = 2\pi\left(\frac{b}{a^{1/4}}\right) \tag{15}$$

and is the characteristic smoothing length of the filter.

[37] We note that variations in the parameters a and b produce quite different changes in the filter pattern, which allows us to separately estimate these parameters from the shoreline elevation pattern. In particular, the partial derivatives of the filter with respect to parameters a and b have the form

$$\begin{bmatrix} \partial/\partial a \\ \partial/\partial b \end{bmatrix} \bar{F}(a,b,k) = -\begin{bmatrix} 1 \\ 4b^3k^4 \end{bmatrix} \bar{F}(a,b,k)^2 \tag{16}$$

The factor of k^4 multiplying the b derivative makes it much larger at high spatial frequencies. That implies that the deflection pattern is much more sensitively dependent on elastic plate thickness at short wavelengths than at long wavelengths, and has greater sensitivity to elastic plate thickness than to substrate density at spatial frequencies above the transition value k_t.

[38] For this model, the spatial-domain impulse response function is also quite simple. The response to a point load is given in terms of Kelvin functions [*Wyman*, 1950; *Yu*, 1957; *Kerr*, 1978; *McNutt and Menard*, 1978; *Lambeck and Nakiboglu*, 1980; *Wolf*, 1984]

$$F(a,b,r) = -\frac{k_t^2}{2\pi}\mathrm{kei}(0, k_t\, r) \tag{17}$$

where r is the radial distance from the load.

[39] If we have a set of shoreline elevations, reasonably well distributed about the lake basin, we can readily estimate the filter parameters a and b which best reproduce the relationship between the spatial patterns of water load and inferred deformation. Note that this is a purely geometrical exercise: We are relating one spatial pattern (the water load) to another spatial pattern (the shoreline deformation). The assumption, at this point, is that the deformation is effectively instantaneous, and that temporal complexities can be ignored.

[40] The parameters we directly recover are themselves purely geometrical. The amplitude and smoothness of the rebound pattern, when compared to that of the load pattern, determine values of the filter parameters a and b which best relate those patterns. It is only secondarily, through the relations 4, 12, and 13, that we recover the physical parameters which are of primary scientific interest. If we had assumed that the density of the fluid filling the lake was 2000 kg m^{-3}, rather than the 1000 kg m^{-3} we actually assumed, then we would recover estimates of the substrate density and plate flexural parameter D twice as large, but the geometrical filter parameters a and b would be exactly the same.

[41] Reconstruction of the lake load is a relatively simple operation. We assume that the present topography in the basin is very nearly the same as it was during the time of shoreline formation, except for the linear superposition of the lake-induced deformation pattern. Our initial estimate of lake water depth simply compares the digitized version of the current topography with an initial estimate of the water surface elevation at the time of shoreline formation. At each point in the topography array, we compare the topographic height with the lake level, and if the lake level is higher than the topography, the load at that point is equal to the difference in elevations. If the topography is higher, there is no load at that point. Using our initial estimate of the load, and an assumed value for the filter parameters, we compute a deformation pattern. We then add that pattern to the present topography and extract a revised load. This process converges quickly, and we have found that three iterations yield a reliable load estimate.

[42] All of the physical models we consider are linear. That is, the computed surface deflection is a linear function of the applied load. However, the load is a nonlinear function of the basin topography and lake surface elevation. As a result, the mapping between topography and deformation is weakly nonlinear.

[43] The approach we follow for estimating the parameters is dominantly carried out in the spatial domain. That is, the load is estimated from the present topography and an initial estimate of water surface elevation. The load is then Fourier transformed and multiplied by a filter array corresponding to a trial set of parameters, $\{a, b\}$. The filtered load is then inverse transformed and compared to the spatial pattern of observed shorelines. At each iteration, the topography array is adjusted by adding the computed deflection pattern, and the lake level is adjusted to make the mean of the observed and computed shoreline elevations agree. Using this approach, we have modeled the Lahontan shoreline deformation pattern and found that it is reasonably well reproduced with an elastic plate model with parameters h = 19.8 km and ρ_s = 3070 kg m^{-3}. The corresponding values of the elastic filter parameters are a = 3.07 and b = 53.0 km. Figure 2 shows the resulting deformation pattern. We examined values in the range

$$16 \text{ km} \le h < 24 \text{ km} \tag{18}$$

$$2800 \text{ kg m}^{-3} \le \rho_s \le 3400 \text{ kg m}^{-3}. \tag{19}$$

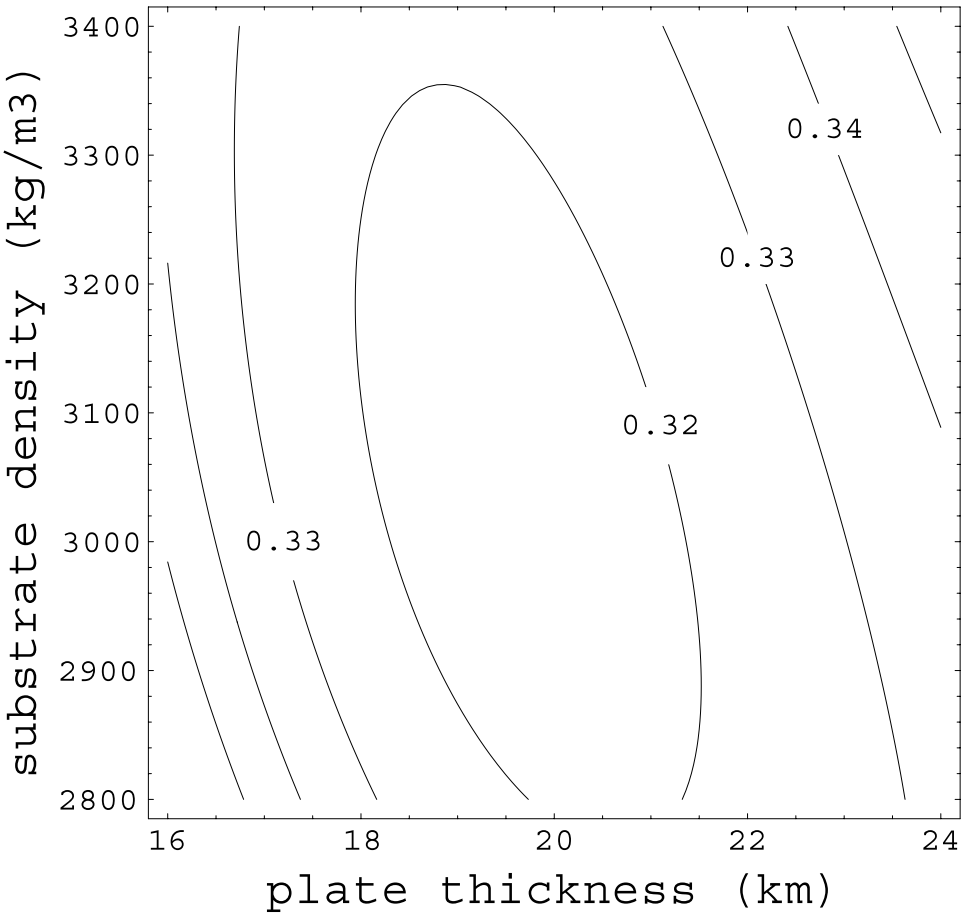

Figure 7. Misfit of elastic model to observation, as parameters h and ρ_s are varied. Contours are labeled with values of residual variance divided by data variance. See discussion in text.

Over that range, the residual variance is a smooth function of the parameter values, as is shown in Figure 7. The best fitting model yields a residual variance of 6.85 m^2 or 31.9% of the data variance.

[44] Our ability to separately estimate the parameters a and b, or alternatively h and ρ_s, is a result of their different influences on the spatial pattern of deformation. Not surprisingly, there is some trade-off between the two parameters. An increase in substrate density, for example, would require a decrease in plate thickness to produce the same maximum deflection value. In our effort to match the full observed spatial pattern of shoreline elevations as well as possible, using the rather convoluted water load makes the effects of these two input parameters quite separable. Writing the deformation pattern w as a convolution of the water depth pattern d with the deflection Green's function F,

$$w(x,y) = F(a,b,r) * d(x,y) \tag{20}$$

the partial derivatives of deformation with respect to parameters a and b are

$$\frac{\partial w}{\partial a} = \frac{\partial F(a,b,r)}{\partial a} * d(x,y) \tag{21}$$

$$\frac{\partial w}{\partial b} = \frac{\partial F(a,b,r)}{\partial b} * d(x,y) \tag{22}$$

4. Viscoelastic Model

[45] To obtain information about the long-term strength of the crust and upper mantle from the shoreline deformation pattern, we must resort to a more complex physical model. The model we have chosen to use in the present analysis is very similar to that previously applied to Lake Bonneville [*Bills et al.*, 1994a]. The Earth model consists of a stack of Maxwell viscoelastic plates, overlying a Maxwell half-space. Each layer is specified by six parameters; upper and lower depth limits, density ρ, rigidity μ, bulk modulus K, and viscosity η. The lake-level history is approximated by a piecewise linear function of time, and the load at each time step is computed from the lake-surface level and present topography pattern in the same way as was done for the elastic model.

[46] The only substantial change from our previous modeling approach, as used for Lake Bonneville, is that we now adjust both the density and viscosity in each layer. We use a starting model with density ρ, rigidity μ, and bulk modulus K specified from seismic observations. There is insufficient information in the shoreline pattern to derive all

the needed parameter values from that source alone. However, because changes in density and changes in viscosity within a given layer will influence the computed pattern of deformation differently, we can at least partially resolve both parameters. Our initial estimates of elastic parameters are taken from the work of *Priestley et al.* [1980].

[47] The elastic parameters are derived from observations of seismic wave traveltimes. The basic observations are of propagation speeds V_p and V_s of compressional and shear waves, respectively. These wave speeds are related to the physical parameters of interest via

$$V_p^2 = \frac{K + 4\mu/3}{\rho} \qquad V_s^2 = \frac{\mu}{\rho} \tag{23}$$

If we are to change the density in a layer by an amount $\Delta\rho$, then in order to keep the wave speeds at their seismically determined values, we need to change K and μ by proportional amounts

$$\frac{\Delta K}{K} = \frac{\Delta\mu}{\mu} = \frac{\Delta\rho}{\rho} \tag{24}$$

We will find, in any event, that the required changes in density structure are quite small.

[48] There are two obvious advantages to adjusting the initial density structure. The first advantage is that adjusting the density allows us to fit the observed pattern of shoreline elevations quite well without recourse to rather artificial quadratic trend surface adjustments, as was done for Lake Bonneville [*Bills et al.*, 1994a]. The second advantage is that it provides a criterion for judging the internal consistency of proposed loading models. That is, the density structure obtained in fitting the elevation pattern might include a density inversion. Since that is not a stable configuration, it clearly signals an inconsistency in the model. We will exploit this property in examining our three candidate loading models. We also advocate the application of a similar approach in future global estimates of viscosity structure from glacial rebound observations.

[49] It is important to note that the parameters we are estimating, in this algorithm, are not the standard temperature and pressure values of the material properties. Rather, they are the in situ values before the water load is applied. Thus for example, the density variations with depth may be due to compositional change or self-compression, or some combination thereof. All that matters for the estimation is the influence of the parameters of interest on the response of the Earth's surface to the applied water load. If there is a density increase with depth, across a layer interface, gravitational restoring forces will impede deformation of that interface. If a layer has high values of rigidity and viscosity, it will be difficult to bend. Though our model does include finite compressibility, the water load is small enough, compared to lithostatic pressure, that there is very little difference in response between compressible and completely incompressible models.

[50] Another caveat, in regards to estimating density structure and using it as a criterion for judging the validity of the input loading history, is that we have no guarantee that our recovered structure model is unique. All that we know, for certain, is that the model produces a local minimum in the residual variance.

[51] In a viscoelastic model, there is a significant trade-off between loading history and inferred viscosity structure. To produce a large amount of deformation, one requires either a low-viscosity region or a long duration of loading. If a load is rapidly emplaced on the surface, there is an initial elastic response and then an exponential approach to a buoyant asymptotic response. Because of the exponential behavior in time and space of the viscoelastic response to surface loading, our ability to resolve density and viscosity structure decreases with increasing depth in an approximately exponential fashion.

[52] The ratio of viscosity to rigidity yields a time constant, the Maxwell time, which characterizes the time required for strain accumulated via viscous flow to match that due to initial elastic deformation. It is an intrinsic material property and can be useful in determining whether elastic or viscous effects are more important on a given timescale. However, it can be somewhat misleading when applied to a structure such as our layered Earth models, in which both rigidity and viscosity are varying with depth. In particular, a structure comprising a stack of viscoelastic layers will exhibit a spectrum of relaxation times. The minimum relaxation time is never less than the lowest single-layer Maxwell time, but can be considerably greater. This issue is discussed at greater length by *Bills and May* [1987].

[53] The simplest model of the type we are now considering would consist of a high viscosity plate on a lower viscosity substrate. In the limit of infinite viscosity in the plate and zero viscosity in the substrate, this model reverts to the buoyantly supported elastic plate model of the previous section. We have examined a wide range of model configurations, with the number of layers varying from 2 to 20. With too few layers, we are not able to fit the observations adequately. With too many layers, the model parameters become poorly constrained. As something of a compromise, we present the results of a model with intermediate complexity.

[54] We have somewhat arbitrarily selected, for detailed presentation here, a series of models with eight layers, consisting of seven plates overlying a semi-infinite substrate. We consider three such models, each one associated with a different loading history. The bounding depths were chosen to be {0, 10, 20, 40, 80, 160, 320, and 640} km, and the elastic parameters were interpolated from the model of *Priestley et al.* [1980]. An initial viscosity profile was chosen which has very high values in the near surface regions, and then decreases rapidly to 3×10^{19} Pa s below 40 km. A total of 19 parameters were adjusted in the fitting process. The adjusted parameters are the densities and viscosities in each layer, the elevation of the lake surface at the time of presumed maximum depth, and two regional slope parameters, which account for any long wavelength deformation of the basin. If there were tectonic deformations in the area, independent of the response to lake loading, we might expect the observed pattern to exhibit a residual tilt. The lake surface elevation, at the time of shoreline formation, is approximately specified by our

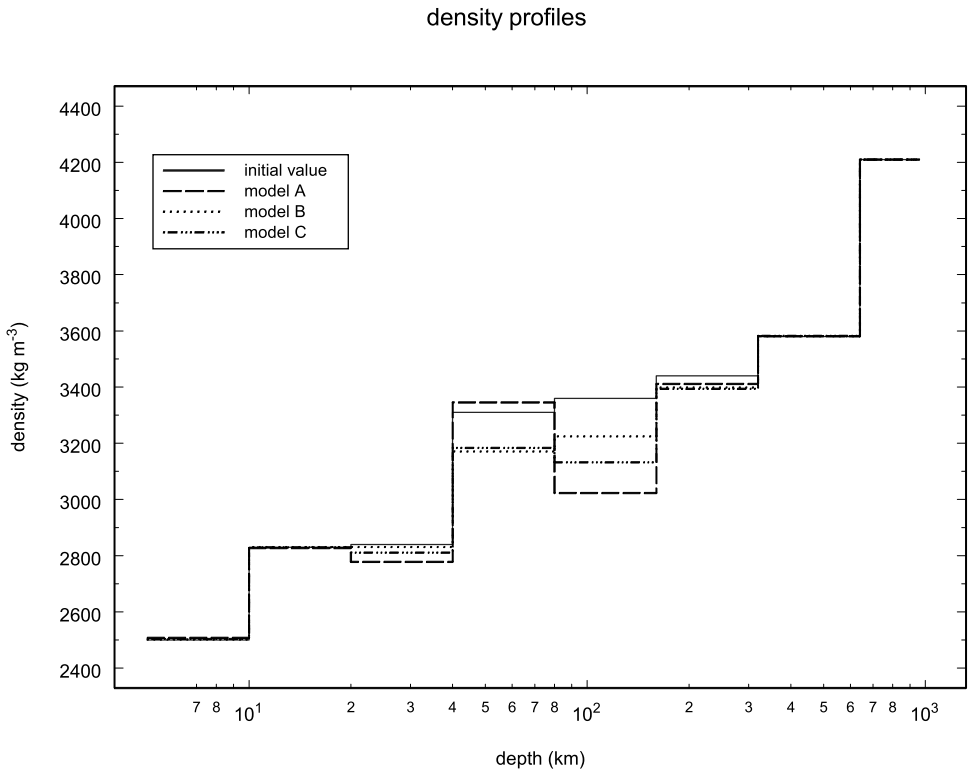

Figure 8. Density structure. The initial density model and those derived from the indicated loading histories are shown as functions of depth.

assumed loading model, as shown in Figure 5. However, to minimize the misfit between observed elevations and model results, we adjust the water level at that time to a value such that the mean residual at the survey locations is zero.

[55] In the case of the elastic plate model, it was relatively simple to do a grid search through a plausible range of parameter values. In the present situation, with a 19-dimensional parameter space, that is not feasible. Instead, we performed a linearized least squares inversion. Linearizing about initial estimates of each of the parameters, we computed the partial derivative of the deflection at each observation point with respect to each of the parameters. The residual elevations Δz are related to parameter changes Δp via

$$\Delta z_i = \sum_j A_{ij} \Delta p_j \tag{25}$$

where the partial derivative matrix is

$$A_{ij} = \frac{\partial z_i}{\partial p_j} \tag{26}$$

The least squares estimate of required parameter changes is then

$$\Delta p = (A^t \cdot A)^{-1} (A^t \cdot \Delta z) \tag{27}$$

As the relationship is now weakly nonlinear, we need to repeat this perturbation estimation step several times.

[56] Figures 8 and 9 compare the recovered density and viscosity profiles for the three loading histories. The best fit obtained with this model was a residual variance of 4.29 m^2, or 19.9% of the data variance. The RMS misfit is thus 2.07 m, which is essentially equal to our estimate of the error in the shoreline elevations. This is a better fit, in absolute terms, but worse in relative terms, than was found for Lake Bonneville by *Bills et al.* [1994a].

[57] Our primary loading history model, which is designated model B and represents the work of *Benson et al.* [1995, 1996], produced the best fit to the data. Our model A, which was a very simplified version of the loading history, performed only slightly worse, at 4.46 m^2. However, as may be seen in Figure 7, it produced a density structure which includes an inversion, with the density in the depth range from 80 to 160 km lower than in the region above. This is not a plausible result, as it would be gravitationally unstable, and we take it to indicate that the loading history is in error.

[58] Our loading model C, which was based on model B, but with minor modifications as described in section 2 above, also performed quite well in fitting the observations, with a residual variance of 4.42 m^2. However, it too produced a density inversion and thus seems to require modification. All three loading models produced density structures in which the primary departure from the starting model was a decrease in density over the depth range from 40 to 160 km. Model B required similar small (~4%) reductions in both the 40–80 and the 80–160 km layers, whereas the other two loading histories required larger adjustments to the density in the lower depth range and

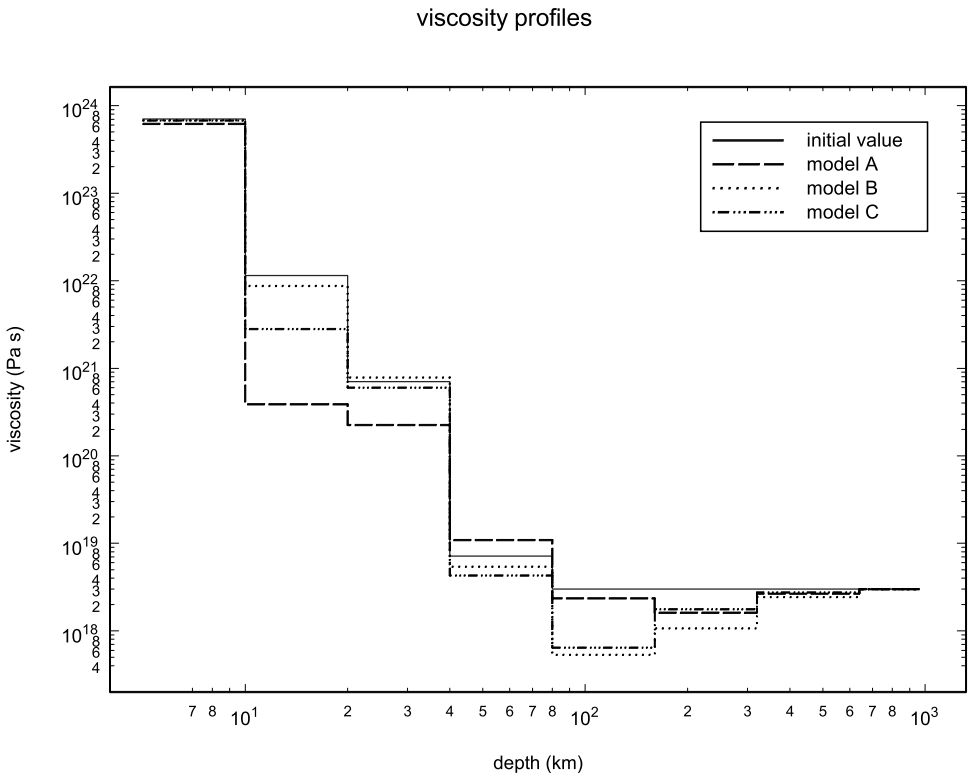

Figure 9. Viscosity structure. The initial viscosity model and those derived from the indicated loading histories are shown as functions of depth.

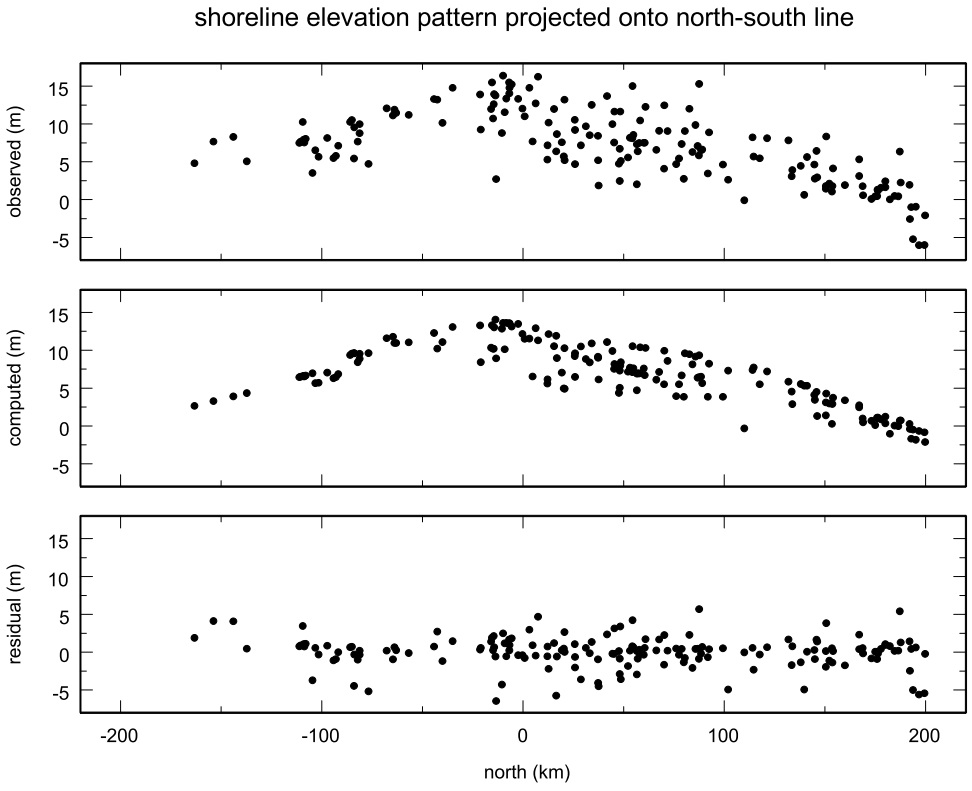

Figure 10. Observed, computed, and residual shoreline elevations projected onto a north-south line.

yielded inversions. From that perspective, they all performed somewhat similarly. However, we reject the models that yield density inversions.

[59] All three loading models yield viscosity profiles which decrease rapidly with depth, attain minimum values in the 80- to 160-km-depth interval, and then increase slightly at greater depths. There is very little change, compared to the initial viscosity values, in the shallowest and deepest layers. However, that mainly reflects low sensitivity in those regions. In the top layer, the viscosity is high enough to be effectively infinite on the $\sim 10^4$-year lake loading timescales. In the deepest layers, the depth is becoming comparable to the longest wavelengths in the load.

[60] When comparing these results with viscosity values estimated for the Bonneville basin [*Bills et al.*, 1994a, Figure 12], the largest difference is the shape of the curve. The Bonneville profile has a very large drop in viscosity, from 10^{21} to 10^{18} Pa s, at 40-km depth, and a return to higher values (3×10^{20} Pa s) at 160 km. The Lahontan profiles are more gradual. The lowest viscosity value attained in the profile associated with the model B loading history is 5×10^{17} Pa s, comparable to the Bonneville minimum.

[61] It is informative to examine the spatial pattern of the misfit between models and data. The mean of the 170 observed elevations is 1331.46 m. The water surface elevation required to make the model deflections match the observed elevations is 1324.43 m. If we subtract that value from each of the observed heights, they will yield local estimates of the cumulative vertical deformation since formation of that shoreline. Using the loading model B, which produced the best fit to the observations, we have made several spatial comparisons. Figure 10 illustrates the spatial patterns of the observed, computed, and residual elevations, with each of them projected onto a N-S line. In

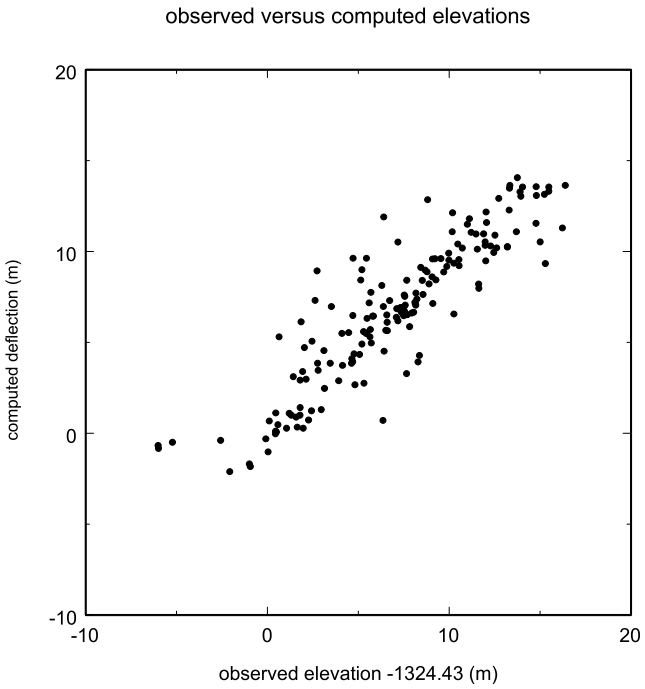

Figure 12. Comparison of observed and computed elevations at each of 170 measurement sites.

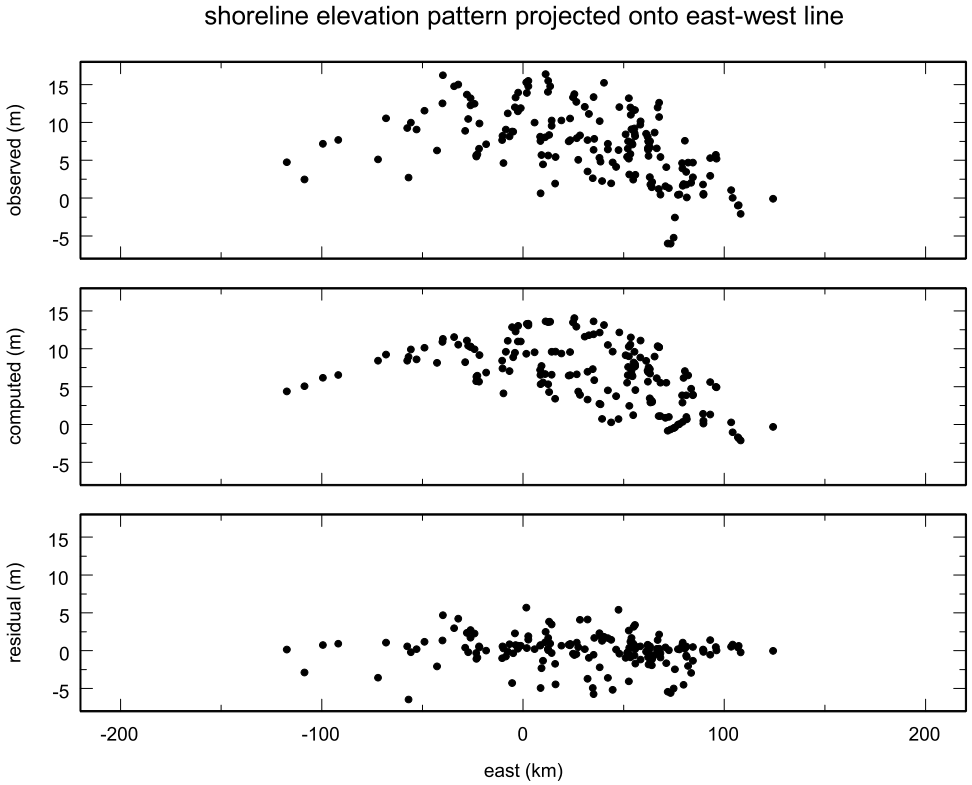

Figure 11. Observed, computed, and residual shoreline elevations projected onto an east-west line.

similar fashion, Figure 11 shows the same quantities, but with a projection onto an E-W line. The main conclusion is that there is no obvious systematic trend in the residuals. If we had a much higher density sampling of the rebound pattern, it might well be evident that patterns of faulting contribute to the misfit. However, with the present data set, we see that the observed elevations are in good, but not perfect, agreement with a simple rebound model.

[62] Figure 12 is a direct comparison between observed and computed deflection values. If the model were perfect, and there were no other sources of vertical motion of shorelines, then the points should all fall on a straight line with unit slope. The model estimates of vertical motion include both the response of the layered viscoelastic model to the imposed water load and inferred regional slope values of $\{-7.01, -12.59\} \times 10^{-6}$ in the east and north directions. The north-south component amounts to a total of roughly 4-m elevation change between the extreme northern and southern extents of the basin. It had been noted earlier [*Adams et al.*, 1999] that the elevations of the northernmost set of shoreline points, in each of several valleys, are lower in elevation than would be expected from a local trend analysis. This effect is clearly seen in the upper panel of Figure 9. The physical explanation for this pattern is still not clear, though it might be related to tectonics associated with the Yellowstone hot spot [*Smith and Braile*, 1994].

5. Discussion

[63] We have used the basinwide pattern of elevations on the highest of the late Pleistocene shorelines in the Lahontan basin of western Nevada to estimate viscosity structure in the crust and upper mantle. On the basis of other evidence, which implies higher temperatures in the upper mantle in that region, it was anticipated that the viscosity beneath the western Great Basin would be even lower than has been found under Lake Bonneville, in the eastern Great Basin. Our results suggest that the situation is somewhat more complicated. Both eastern and western Great Basin viscosity estimates are dramatically lower than global upper mantle average values of 10^{21} Pa s, as inferred from numerous glacial rebound studies. The minimum viscosity values under Bonneville and Lahontan are both roughly 5×10^{17} Pa s, but the low-viscosity region under Bonneville is more sharply defined. It has rather abrupt transitions, with a decrease at 40-km depth and an increase at 160-km depth. In contrast, the Lahontan profile decreases more gradually with depth and does not increase as much at great depth.

[64] Viscosity values for rocks of the crust and upper mantle are expected to vary with composition, temperature, and pressure [*Karato and Wu*, 1993; *Hirth and Kohlstedt*, 1996; *Williams*, 1996; *Dixon et al.*, 2004]. As both temperature and pressure are expected to be rather smooth functions of depth, an abrupt drop in viscosity, as is seen in the Bonneville results, would suggest a corresponding compositional change. However, it occurs below the seismically determined crust-mantle interface [*Smith and Bruhn*, 1984].

[65] If we assume that the low-viscosity regions in the upper mantle are mainly controlled by temperature, this would suggest that high temperatures exist at shallower depths beneath Lahontan than beneath Bonneville. The higher heat flow in the western Great Basin certainly reflects a steeper temperature gradient across the thermal boundary layer. However, from the heat flow data alone, it is not possible to say whether the steeper gradient in the west persists to great depth. The similarity of the minimum inferred viscosities beneath the eastern and western portions of the Great Basin suggests that the temperatures at 100-km depth, for example, are quite similar in the two regions, though the temperatures at 40-km depth might be quite different.

[66] The very low values inferred for upper mantle viscosity beneath Utah and Nevada are similar to the values derived from postseismic deformation associated with a number of earthquakes in southern California [*Pollitz et al.*, 2000]. They are also similar to the values in an oceanic asthenosphere as inferred from models of oceanic ridge morphology [*Yale and Morgan*, 1998; *Albers and Christensen*, 2001] and from observations of deformation in Iceland [*Sigmundsson and Einarsson*, 1992; *Pollitz and Sacks*, 1996; *Sjoberg et al.*, 2000, 2004]. *Kaufmann and Amelung* [2000] also found an effective viscosity of $\sim 10^{18}$ Pa s in southern Nevada, from modeling the deflection associated with the filling of Lake Mead. In this regard, the tectonically active western part of North America appears more oceanic than cratonic.

[67] We have employed a new algorithm for estimating viscosity structure, in which we adjust both the viscosity and the density in each layer. The resulting density structure remains close to that inferred from seismic observations, but allows a better fit to the data, and potentially reveals problems in the loading history. A similar approach should be applied in future inversions for global viscosity structure from postglacial rebound observations.

[68] Better resolution of the viscosity structure beneath Lake Lahontan would be quite informative and could be readily obtained by application of the algorithms used here to an extended data set. Our primary data needs are geometric and chronologic. The geometric constraints are easily obtainable. All that is needed, in that regard, are surveyed elevations of some of the many lower shorelines. The temporal constraints will likely take more effort. There is need for more samples of datable material in appropriate stratigraphic contexts in order to place better constraints on the lake surface elevation history. Finding them will take effort but should be pursued.

[69] **Acknowledgments.** Portions of this work were supported by NSF grant EAR-9405057. We benefited from insightful reviews by Detlef Wolf, Bert Vermeersen, and Georg Kaumann.

References

Adams, K. D., and S. G. Wesnousky (1998), Shoreline processes and the age of Lake Lahontan highstand in the Jessup embayment, *Bull. Geol. Soc. Am.*, *110*, 1318–1332.

Adams, K. D., S. G. Wesnousky, and B. G. Bills (1999), Isostatic rebound, active faulting, and potential geomorphic effects in the Lake Lahontan basin, Nevada and California, *Bull. Geol. Soc. Am.*, *111*, 1739–1756.

Albers, M., and U. R. Christensen (2001), Channeling of plume flow beneath mid-ocean ridges, *Earth Planet. Sci. Lett.*, *187*, 207–220.

Argollo, J., and P. Mourguiart (2000), Late Quaternary climate history of the Bolivian Altiplano, *Quat. Int.*, *72*, 37–51.

Baker, P. A., C. A. Rigsby, G. O. Seltzer, S. C. Fritz, T. K. Lowenstein, N. P. Bacher, and C. Veliz (2001), Tropical climate changes at millennial and orbital timescales on the Bolivian Altiplano, *Nature*, *409*, 698–701.

Beck, J. W., D. A. Richards, R. L. Edwards, B. W. Silverman, P. L. Smart, D. J. Donahue, S. Hererra-Osterheld, G. S. Burr, L. Calsoyas, A. J. T. Jull, and D. Biddulph (2001), Extremely large variations of atmospheric

C-14 concentration during the last glacial period, *Science*, *292*, 2453–2458.
Bennette, R. A., B. P. Wernicke, and J. L. Davis (1998), Continuous GPS measurements of contemporary deformation across the northern Basin and Range province, *Geophys. Res. Lett.*, *25*, 563–566.
Benson, L. V., and R. A. Thompson (1987), Lake level variation in the Lahontan basin for the past 50,000 years, *Quat. Res.*, *28*, 69–85.
Benson, L. V., P. A. Meyers, and R. J. Spencer (1991), Change in the size of Walker Lake during the past 5000 years, *Palaeogeogr., Palaeoclimatol., Palaeoecol.*, *81*, 189–214.
Benson, L. V., D. R. Currey, Y. Lao, and S. W. Hostetler (1992), Lake-size variations in the Lahontan and Bonneville basins between 13,000 and 9,000 (super 14) C yr B. P., *Palaeogeogr., Palaeoclimatol., Palaeoecol.*, *95*(1–2), 19–32.
Benson, L. V., M. Kashgarian, and M. Rubin (1995), Carbonate deposition, Pyramid Lake subbasin, Nevada. 2. Lake levels and polar-jet stream positions reconstructed from radiocarbon ages and elevations of carbonates (tufas) deposited in the Lahontan basin, *Palaeogeogr., Palaeoclimatol., Palaeoecol.*, *117*, 1–30.
Benson, L. V., L. D. White, and R. Rye (1996), Carbonate deposition, Pyramid Lake Subbasin, Nevada. 4. Comparison of the stable isotope values of carbonate deposits (tufas) and the Lahontan lake-level record, *Palaeogeogr., Palaeoclimatol., Palaeoecol.*, *119*, 201–213.
Benson, L. V., J. P. Smoot, M. Kashgarian, W. A. M. Sarna, and J. W. Burdett (1997), Radiocarbon ages and environments of deposition of the Wono and Trego Hot Springs tephra layers in the Pyramid Lake subbasin, Nevada, *Quat. Res.*, *47*, 251–260.
Bills, B. G., and G. M. May (1987), Lake Bonneville: Constraints on lithospheric thickness and upper mantle viscosity from isostatic warping of Bonneville, Provo, and Gilbert stage shorelines, *J. Geophys. Res.*, *92*, 11493–11508.
Bills, B. G., D. R. Currey, and G. A. Marshall (1994a), Viscosity estimates for the crust and upper-mantle from patterns of shoreline deformation in the Eastern Great-Basin, *J. Geophys. Res.*, *99*, 22,059–22,086.
Bills, B. G., S. L. de Silva, D. R. Currey, R. S. Emenger, K. D. Lillquist, A. Donnellan, and B. Worden (1994b), Hydro-isostatic deflection and tectonic tilting in the Central Andes: Initial results of a GPS survey of Lake Minchin shorelines, *Geophys. Res. Lett.*, *21*, 293–296.
Bills, B. G., T. J. Wambeam, and D. R. Currey (2002), Geodynamics of Lake Bonneville, in Great Salt Lake: An overview of change, in Utah Geol. Surv. Special Pub., edited by J. W. Gwynn, pp. 14–32.
Bluck, B. J. (1967), Sedimentation of beach gravels: Examples from South Wales, *J. Sediment. Petrol.*, *37*, 125–156.
Born, S. M. (1972), *Late Quaternary History, Deltaic Sedimentation, and Mudlump Formation at Pyramid Lake, Nevada*, 97 pp., Center for Water Resources, Desert Research Institute, Reno, Nevada.
Bradbury, J. P., R. M. Forester, and R. S. Thompson (1989), Late Quaternary paleolimnology of Walker Lake, Nevada, *J. Paleolimnol.*, *1*, 249–267.
Briggs, R. W., S. G. Wesnousky, and K. D. Adams (2005), Late pleistocene and late holocene lake highstands in the Pyramid Lake subbasin of Lake Lahontan, Nevada, USA, *Quat. Res.*, *64*, 257–263.
Buckles, J. E., K. Kashiwase, and T. Krantz (2002), Reconstruction of prehistoric Lake Cahuilla in the Salton Sea basin using GIS and GPS, *Hydrobiologia*, *473*, 55–57.
Carter, R. W. G., and J. D. Orford (1988), Conceptual models of coarse clastic barrier formation from multiple sources, *Geogr. Rev.*, *78*, 221–239.
Caskey, S. J., and A. R. Ramelli (2004), Tectonic displacement and far-field isostatic flexure of pluvial lake shorelines, Dixie Valley, Nevada, *J. Geodyn.*, *38*, 131–145.
Crittenden, M. D. (1963), Effective viscosity of the Earth derived from isostatic loading of Pleistocene Lake Bonneville, *J. Geophys. Res.*, *68*, 5517–5530.
Currey, D. R. (1982), Lake Bonneville: Selected features of relevance to neotectonic analysis, U.S. Geol. Surv. Open File Rep. 82-1070, 31 pp.
Dansie, A. J., J. O. Davis, and T. W. Stafford (1988), The Wizards Beach Recession: Farmdalian (25,500 yr B.P.) vertebrate fossils co-occur with early Holocene artifacts, in *Early Human Occupation in Far Western North America: The Clovis-Archaic Interface*, edited by J. A. Willig, C. M. Aikens, and J. L. Fagan, pp. 153–200, Nevada State Museum Anthropological Papers Number 21, Carson City, Nevada.
Davis, J. O. (1983), Level of Lake Lahontan during deposition of the Trego Hot Springs Tephra about 23,400 years ago, *Quat. Res.*, *19*, 312–324.
Davis, J. O. (1985), Correlation of late Quaternary tephra layers in a long pluvial sequence near Summer Lake, Oregon, *Quat. Res.*, *23*, 38–53.
Davis, J. O. (1987), *Introduction to the Pleistocene Geology of Northwestern Lake Lahontan, Nevada*, 28 pp., Friends of the Pleistocene Pacific Cell fieldtrip guidebook, Reno, Nevada.
DePaolo, D. J., and E. E. Daley (2000), Neodymium isotopes in basalts of the southwestern basin and range and thinning during continental extension, *Chem. Geol.*, *169*, 157–185.
Dillon, W. P. (1971), Submergence effects on a Rhode Island barrier and lagoon and influence on barrier migration, *J. Geol.*, *78*, 94–106.
Dixon, T. H., S. Robaudo, J. Lee, and M. C. Reheis (1995), Constraints on present-day Basin and Range deformation from space geodesy, *Tectonics*, *14*, 755–772.
Dixon, J. E., T. H. Dixon, D. R. Bell, and R. Malservisi (2004), Lateral variation in upper mantle viscosity: Role of water, *Earth Planet. Sci. Lett.*, *222*, 451–467.
Farmer, G. L., and T. T. Ball (1997), Sources of Middle Proterozoic to Early Cambrian siliciclastic sedimentary rocks in the Great Basin: A Nd isotope study, *Geol. Soc. Am. Bull.*, *109*, 1193–1205.
Forbes, D. L., R. B. Taylor, J. D. Orford, R. W. G. Carter, and J. Shaw (1991), Gravel barrier migration and overstepping, *Mar. Geol.*, *97*, 305–313.
Fornari, M., F. Risacher, and G. Feraud (2001), Dating of paleolakes in the central Altiplano of Bolivia, *Palaeogeogr., Palaeoclimatol., Palaeoecol.*, *172*, 269–282.
Ghienne, J. F., M. Schuster, A. Bernard, P. Duringer, and M. Brunet (2002), The Holocene giant Lake Chad revealed by digital elevation models, *Quat. Int.*, *87*, 81–85.
Gilbert, G. K. (1890), Lake Bonneville, U.S. Geological Survey Monograph 1, 438 pp.
Grunert, J., F. Lehmkuhl, and M. Walther (2000), Paleoclimatic evolution of the Uvs Nurr basin and adjacent areas (western Mongolia), *Quat. Int.*, *65*, 171–192.
Hare, J. L., J. F. Ferguson, C. L. V. Aiken, and J. S. Oldow (2001), Quantitative characterization and elevation estimation of Lake Lahontan shoreline terraces from high-resolution digital elevation models, *J. Geophys. Res.*, *106*, 26,761–26,774.
Hirth, G., and D. L. Kohlstedt (1996), Water in the oceanic upper mantle: Implications for rheology, melt extraction and the evolution of the lithosphere, *Earth Planet. Sci. Lett.*, *144*, 93–108.
Humphreys, E. D., and K. G. Dueker (1994a), Western U.S. upper mantle structure, *J. Geophys. Res.*, *99*, 9615–9634.
Humphreys, E. D., and K. G. Dueker (1994b), Physical state of the western U.S. upper mantle, *J. Geophys. Res.*, *99*, 9635–9650.
Iwasaki, T., and M. Matsuura (1982), Quasi-static crustal deformations due to a surface load: Rheological structure of the Earth's crust and upper mantle, *J. Phys. Earth*, *30*, 469–508.
Karato, S. I., and P. Wu (1993), Rheology of the upper mantle: A synthesis, *Science*, *260*, 771–778.
Kaufmann, G., and F. Amelung (2000), Reservoir-induced deformation and continental rheology in vicinity of Lake Mead, Nevada, *J. Geophys. Res.*, *105*, 16,341–16,358.
Kaufmann, G., and K. Lambeck (2000), Mantle dynamics, postglacial rebound and the radial viscosity profile, *Phys. Earth Planet. Inter.*, *121*, 301–324.
Kerr, A. D. (1978), An indirect method of evaluating certain infinite integrals, *J. Appl. Math. Phys.*, *29*, 380–386.
King, G. Q. (1993), Late Quaternary history of the lower Walker river and its implications for the Lahontan paleolake system, *Phys. Geogr.*, *14*, 81–96.
Kirk, R. M. (1975), Aspects of surf and run-up processes on mixed sand and gravel beaches, *Geogr. Ann.*, *57*, 117–133.
Kirk, R. M. (1980), Mixed sand and gravel beaches: morphology, processes and sediments, *Prog. Phys. Geogr.*, *4*, 189–210.
Komatsu, G., P. J. Brantingham, J. W. Olsen, and V. R. Baker (2001), Paleoshoreline geomorphology of Boon Tsagaan Nuur, Tsagaan Nuur and Orog Nurr: the Valley of Lakes, Mongolia, *Geomorphology*, *39*, 83–98.
Kutzbach, J. E. (1980), Estimates of past climate at paleolake Chad, North Africa, based on a hydrological and energy balance model, *Quat. Res.*, *14*, 210–223.
Lachenbruch, A. H. (1978), Heat flow in the Basin and Range province and thermal effects of tectonic extension, *Pure Appl. Geophys.*, *117*, 34–50.
Lambeck, K., and S. M. Nakiboglu (1980), Seamount loading and stress in the oceanic lithosphere, *J. Geophys. Res.*, *85*, 6403–6418.
Lambert, A., J. O. Liard, and A. Mainville (1986), Vertical movement and gravity change near the La Grande-2 reservoir, Quebec, *J. Geophys. Res.*, *91*, 9150–9160.
Larson, K. M. (1990), Precision, Accuracy, and Tectonics from the Global Positioning System, Ph.D. dissertation, pp. 230–261, University of California, San Diego.
Lehmkuhl, F., and F. Haselein (2000), Quaternary paleoenvironmental change on the Tibetan Plateau and adjacent areas (western China and western Mongolia), *Quat. Int.*, *65*, 121–145.

Lehmkuhl, F., and A. Lang (2001), Geomorphological investigations and luminescence dating in the southern part of the Khangay and the valley of the Gobi Lakes (Central Mongolia), *J. Quat. Sci.*, *16*, 69–87.

Lowry, A. R., and R. B. Smith (1994), Flexural rigidity of the Basin and Range-Colorado Plateau-Rocky Mountain transition from coherence analysis of gravity and topography, *J. Geophys. Res.*, *99*, 20,123–20,140.

Lowry, A. R., and R. B. Smith (1995), Strength and rheology of the western U.S. cordillera, *J. Geophys. Res.*, *100*, 17,947–17,963.

McKee, E. H., and D. C. Noble (1986), Tectonic and magmatic development of the Great Basin of western United States during late Cenozoic time, *Mod. Geol.*, *10*, 39–49.

McNutt, M. K., and H. W. Menard (1978), Lithospheric flexure and uplifted atolls, *J. Geophys. Res.*, *83*, 1206–1212.

Mifflin, M. D. (1984), Paleohydrology of the Lahontan basin, in *Western Geological Excursions*, edited by J. Lintz, vol. 3, pp. 134–137, Mackay School of Mines, Reno, Nevada.

Mifflin, M. D., and M. M. Wheat (1971), Isostatic rebound in the Lahontan basin, northwestern Great Basin, *Geol. Soc. Am. Abstr. Programs*, *3*, 647.

Mifflin, M. D., and M. M. Wheat (1979), Pluvial lakes and estimated pluvial climates of Nevada, Nevada Bureau of Mines and Geology Bulletin 94, 57 pp.

Minster, J. B., and T. H. Jordan (1987), Vector constraints on western U.S. deformation from space geodesy, neotectonics and plate motions, *J. Geophys. Res.*, *92*, 4798–4804.

Mitrovica, J. X., G. A. Milne, and J. L. Davis (2001), Glacial isostatic adjustment on a rotating Earth, *Geophys. J. Int.*, *147*, 562–578.

Morrison, R. B. (1964), Lake Lahontan: Geology of the southern Carson Desert, U.S. Geol. Surv. Prof. Paper 401, 156 pp.

Morrison, R. B. (1991), Quaternary geology of the southern Basin and Range Province, in Quaternary nonglacial geology: Conterminous U.S., edited by R. B. Morrison, *Geol. Soc. Amer.*, pp. 353–371.

Nakiboglu, S. M., and K. Lambeck (1982), A study of the Earth's response to surface loading with application to Lake Bonneville, *Geophys. J. R. Astron. Soc.*, *70*, 577–620.

Nakiboglu, S. M., and K. Lambeck (1983), A reevaluation of the isostatic rebound of Lake Bonneville, *J. Geophys. Res.*, *88*, 439–447.

Olivry, J. C., A. Chouret, G. Vuillaume, J. Lemoalle, and J. P. Bricquet (1996), Hydrologie du lac Tchad. Mono. Hydrolog. ORSTOM, 12, 266 pp.

Orford, J. D., D. L. Forbes, and S. C. Jennings (2002), Organisational controls, typologies and time scales of paraglacial gravel-dominated coastal systems, *Geomorphology*, *48*, 51–85.

Oviatt, C. G., and R. S. Thompson (2002), Recent developments in the study of Lake Bonneville, in Great Salt Lake: An overview of change, Utah Geol. Surv. Special Pub., edited by J. W. Gwynn, pp. 1–6.

Passey, Q. R. (1981), Upper mantle viscosity derived from the difference in rebound of the Provo and Bonneville shorelines: Lake Bonneville basin, Utah, *J. Geophys. Res.*, *86*, 11,701–11,708.

Peck, J. A., P. Khosbayar, S. J. Fowell, R. B. Pearce, S. Ariunbileg, B. C. S. Hansen, and N. Soninkhishig (2002), Mid to Late Holocene climate change in north central Mongolia as recorded in sediments of Lake Telmen, *Palaeogeogr., Palaeoclimatol., Palaeoecol.*, *183*, 135–153.

Peltier, W. R. (1998), The inverse problem for mantle viscosity, *Inverse Probl.*, *14*, 441–478.

Peltier, W. R., I. Shennan, R. Drummond, and B. Horton (2002), On the postglacial isostatic adjustment of the British Isles and the shallow viscoelastic structure of the Earth, *Geophys. J. Int.*, *148*, 443–475.

Pollitz, F. F., and I. S. Sacks (1996), Viscosity structure beneath northeast Iceland, *J. Geophys. Res.*, *101*, 17771–17793.

Pollitz, F. F., G. Peltzer, and R. Burgmann (2000), Mobility of continental mantle: Evidence from postseismic geodetic observations following the 1992 Landers earthquake, *J. Geophys. Res.*, *105*, 8035–8054.

Priestley, K., J. A. Orcutt, and J. N. Brune (1980), Higher-mode surface-waves and structure of the Great Basin of Nevada and western Utah, *J. Geophys. Res.*, *85*, 7166–7174.

Reheis, M. (1999a), Extent of Pleistocene lakes in the Western Great Basin, U.S. Geol. Surv. Misc. Field Studies MF-2323.

Reheis, M. (1999b), Highest pluvial-lake shorelines and Pleistocene climate of the Western Great Basin, *Quat. Res.*, *52*, 196–205.

Russell, I. C. (1885), Geological history of Lake Lahontan, a Quaternary lake of northwestern Nevada, U.S. Geological Survey Monograph 11, 288 p.

Sigmundsson, F., and P. Einarsson (1992), Glacio-isostatic crustal movements caused by historical volume change of the Vatnajokull ice cap, Iceland, *Geophys. Res. Lett.*, *19*, 2123–2126.

Sjoberg, L. E., M. Pan, E. Asenjo, and S. Erlingsson (2000), Glacial rebound near Vatnajokul, Iceland, studied by GPS campaigns in 1992 and 1996, *J. Geodyn.*, *29*, 63–70.

Sjobert, L. E., M. Pan, S. Erlingsson, E. Asenjo, and K. Arnason (2004), Land uplift near Vatnajokull, Iceland, as observed by GPS in 1992, 1996 and 1999, *Geophys. J. Int.*, *159*, 943–948.

Smith, R. B., and L. W. Braile (1994), The Yellowstone Hotspot, *J. Volcanol. Geotherm. Res.*, *61*, 121–187.

Smith, R. B., and R. L. Bruhn (1984), Intraplate extensional tectonics of the eastern Basin and Range: Inferences on structural style from seismic reflection data, regional tectonics, and thermal-mechanical models of brittle-ductile deformation, *J. Geophys. Res.*, *89*, 5732–5762.

Stuiver, M., P. J. Reimer, E. Bard, J. W. Beck, G. S. Burr, K. A. Hughen, B. Kromer, G. McCormac, J. vanderPlicht, and M. Spurk (1998), INTCAL98 Radiocarbon Age Calibration, 24000-0 cal BP, *Radiocarbon*, *40*, 1041–1083.

Sturm, R., D. Stow, and T. Rockwell (1996), Mapping Pleistocene-age shoreline deposits in the seismically active Salton Trough using thermal infrared multi-spectral scanner (TIMS) data, *Int. J. Remote Sens.*, *17*, 553–575.

Tackman, G. (1993), Middle and Late Pleistocene hydrologic history of Diamond Valley, Eureka and Elko Counties, Nevada, with climatic and isostatic implications, Geography Dept. Univ. Utah, M.S. thesis, 194 pp.

Timoshenko, S. P., and S. Woinowsky-Krieger (1959), *Theory of Plates and Shells*, McGraw-Hill, New York.

Wang, H. S. (2000), Surface vertical displacements and level plane changes in the front reservoir area caused by filling the Three Gorges Reservoir, *J. Geophys. Res.*, *105*, 13,211–13,220.

Wang, H., H. T. Hsu, and Y. Z. Zhu (2002), Prediction of surface horizontal displacements, and gravity and tilt changes caused by filling the Three Gorges Reservoir, *J. Geod.*, *76*, 105–114.

Waters, M. R. (1983), Late Holocene lacustrine chronology and archaeology of ancient lake Cahuilla, California, *Quat. Res.*, *19*, 373–387.

Watts, A. B. (2001), *Isostasy and Flexure of the Lithosphere*, 478 pp., Cambridge Univ. Press, New York.

Williams, A. T., and N. E. Caldwell (1988), Particle size and shape in pebble-beach sedimentation, *Mar. Geol.*, *64*, 374–399.

Williams, C. F. (1996), Temperature and the seismic/aseismic transition: Observations from the 1992 Landers earthquake, *Geophys. Res. Lett.*, *23*, 2929–2932.

Wolf, D. (1984), On the relation between two-dimensional and axisymmetric loads in plate flexure problems, *J. Geophys.*, *54*, 232–235.

Wyman, M. (1950), Deflection of an infinite plate, *Can. J. Res.*, *A28*, 293–302.

Yale, M. M., and J. P. Morgan (1998), Asthenosphere flow model of hotspot-ridge interactions: A comparison of Iceland and Kerguelen, *Earth Planet. Sci. Lett.*, *161*, 45–56.

Yu, Y. Y. (1957), On the generalized Kelvin functions with applications to plate problems, *Q. J. Mech. Appl. Math.*, *10*, 254–256.

Zhang, K. F., W. E. Featherstone, S. F. Bian, and B. Z. Tao (1996), Time variations of the Earth's gravity field and crustal deformation due to the establishment of the Three Gorges reservoir, *J. Geod.*, *70*, 440–449.

Zoback, M. L. (1989), State of stress and modern deformation of the northern Basin and Range province, *J. Geophys. Res.*, *94*, 7105–7128.

K. D. Adams, Desert Research Institute, Reno, NV, USA.

B. G. Bills, NASA Goddard Space Flight Center, Greenbelt, MD, USA. (bbills@ucsd.edu)

S. G. Wesnousky, Center for Neotectonic Studies, University of Nevada, Reno, NV, USA.